Chemical and biological evaluation of cross-linked halloysite-curcumin derivatives

Marina Massaro, [a]† Paola Poma, [a]† Carmelo G. Colletti, [a] Anna Barattucci, [b] Paola M. Bonaccorsi, [b] Giuseppe Lazzara, [c] Giuseppe Nicotra, [d] Filippo Parisi, [c] Tania M. G. Salerno, [b] Corrado Spinella [d] and Serena Riela*[a]

[a] Dipartimento STEBICEF, Sez. Chimica, Università degli Studi di Palermo, Viale delle Scienze, Ed. 17, 90128 Palermo, Italy. E-mail: serena.riela@unipa.it

[b] Dipartimento di Scienze Chimiche, Biologiche, Farmaceutiche ed Ambientali (ChiBioFarAm) Università di Messina, Viale F. Stagno d'Alcontres 31, Messina, Italy.

[c] Dipartimento di Fisica e Chimica, Università degli Studi di Palermo, Viale delle Scienze, Ed. 17, 90128 Palermo, Italy.

[d] CNR-IMM, Zona Industriale Strada VIII, 5, 95121 Catania, Italy.

† These authors contributed equally

KEYWORDS. Halloysite nanotubes, curcumin derivatives, dual drug delivery, antiproliferative activity, breast cancer cell lines and acute myeloid leukemia cell lines.

ABSTRACT. Well designed and safe nano drug carrier systems are an important tool in biomedical applications. The combination of two or more drugs has been used in medicine both to enhance the therapeutic effect and to decrease the side effects of drugs. Biocompatible halloysite nanotubes, that possess two different surfaces, are a suitable nanomaterial for a simultaneous carrier and release of two drugs that can exert a synergistic effect against cancer cells. In this study, three curcumin derivatives and doxorubicin were loaded by supramolecular and covalent linkage at the lumen and external surface of the halloysite nanotubes. The obtained multifunctional systems were characterized by several techniques and the kinetic release of the drugs from the lumen was also investigated. Finally, the cytotoxic effects of the multifunctional carriers were evaluated on different cancer cell lines, namely breast cancer cell lines (SUM-149 and MDA-MB-231) and acute myeloid leukemia cell lines (HL60 and HL60R). The obtained results show promising cytotoxicity activity of the hybrids which is correlated to the nanoparticles size and to the release profile of the drug supramolecularly loaded on HNT surfaces.

INTRODUCTION. According to the American Institute of Cancer Research there were an estimated 18 million cancer cases around the world in 2018. Cancer represents still a challenging disease, although targeted chirurgical and chemotherapies have extended patients' life expectancy and quality. Some chemodrugs, which kill cancer cells, possess side effects that in the long run can damage normal cells, too. Therefore, the combination of multiple chemotherapeutic agents, that

individually could show low cytotoxicity, has been used in medicine for enhance cancer therapy with a concomitant decrease both in side effects and drug resistance.(Paci et al., 2014)

Unfortunately, chemotherapeutic molecules often show poor aqueous solubility and short lifetime. Several carrier systems, such as micelles, liposomes, and dendrimers, have been developed, to overcome these limitations.(Lin et al., 2019; Pourjavadi et al., 2018; Zhang et al., 2016) Among them, inorganic nanocarriers such as clay minerals are emerging nanomaterials that have been used for biomedical purposes since prehistory.(Bergaya and Lagaly, 2006; Massaro et al., 2018d) Recently, great attention has been attracted by halloysite, a clay mineral of the kaolin group, similar to kaolinite. This clay mineral has been widely used for biomedical applications as nanocontainer(Massaro et al., 2019b; Massaro et al., 2016b) for drug delivery and tissue engineering applications.(Fakhrullin and Lvov, 2016; Yendluri et al., 2017)

Halloysite is an aluminosilicate with a predominantly hollow tubular structure (HNTs). Generally, the inner and outer diameters of the tubes are in the ranges of 10–30 nm and 40–70 nm, respectively, while their length is in the range of 0.2–1.5 μm. Halloysite possesses different charged surfaces: positive in the inner lumen, where mostly of aluminum hydroxide are present; negative in the external one, which consists in silicon dioxide. Due to the different chemical composition, halloysite nanotubes can be selectively functionalized at the inner and/or outer surfaces leading to the synthesis of several interesting nanomaterials.(Massaro et al., 2018b; Massaro et al., 2019c; Massaro et al., 2018c)

Halloysite biological safety has been reported both by *in vitro* and *in vivo* studies.(Bellani et al., 2016; Fakhrullina et al., 2015; Fan et al., 2013; Kryuchkova et al., 2016; Wang et al.) In general, the HNTs are able to penetrate the cellular membrane surrounding the cell nuclei.(Lvov et al., 2014) In addition, it has been proved that the modification of the tube surfaces makes hybrid nanomaterials that penetrate the nucleus membrane, too.(Massaro et al., 2019a) So far, several biologically active molecules were simultaneously loaded onto HNTs obtaining synergistic cytotoxic effects. In our previous studies, we have analyzed the possibility to link, in different ways, curcumin that has shown remarkable antitumoral effects. In particular we have exploited the antiproliferative effects of curcumin both loaded into HNT lumen(Riela et al., 2014) and covalently grafted on the external surface.(Massaro et al., 2016a) In the latter case we have observed enhanced cytotoxicity compared to the supramolecular complex.

Recently, some of us have synthetized and studied, on different cell lines, the antitumoral effects of three curcumin derivatives (Figure 1) that have shown higher antitumor capacities and promising ability to overcame drug resistance with respect to pristine curcumin.(Bonaccorsi et al., 2019) Herein, in order to develop a multifunctional system for the co-delivery of different drugs we report

the synthesis of novel carriers based on the covalent linkage of curcumin derivatives Cur–**1** and Cur–**2** onto the HNT external surface and curcumin derivative Cur–**3** loaded into HNT lumen (Figure 2).

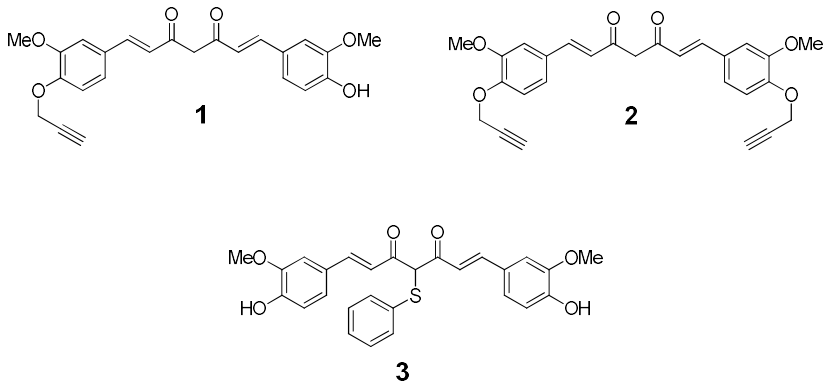

Figure 1. Structure of the investigated curcumin derivatives.

The HNT derivatives were thoroughly investigated by a physico-chemical point of view and the kinetic release was also investigated. Finally, the cytotoxic effects of the multifunctional carriers were evaluated on different cancer cell lines, namely breast cancer cell lines (SUM-149 and MDA-MB-231) and acute myeloid leukemia cell lines (HL60 and HL60R). These cell lines are models of neoplastic disease because are characterized by both innate and acquired high multidrug resistance. In particular, among all breast cancers, the triple-negative breast cancer (TNBC) remain one of the most aggressive and not responsive to common therapies for its high molecular heterogeneity and the lack of estrogen, progesterone and human epidermal growth factor receptor-2 (HER2) receptors. The acute myeloid leukemia, on the contrary, has a good responsiveness to first-line treatments, but soon it acquires resistance to the same treatments. For these reasons cell line HL60 and its multidrug resistant variant HL60R are excellent models of study. The variant HL60R, obtained by HL60 cells after many steps with doxorubicin, is characterized by overexpression of P-glycoprotein, a multidrug transporter, NF-κB and numerous IAPs (Inhibitory of Apoptosis Proteins), exhibiting resistance to apoptosis induced by drugs.

Furthermore, in the case of acute myeloid leukemia cell lines, that did not show response to the HNT-curcumin derivatives, we have investigated the effect of doxorubicin (Dox). It is indeed known that a co-administration of a mixture of doxorubicin and curcumin can reduce the tumor growth and enhance the cancerous cell death, in comparison to the single drugs.(Ma et al., 2017) In addition, it could overcome the multidrug resistance, often associated with the doxorubicin administration and it could be limited the severe side effects, increasing the patience compliance.(Babos et al., 2018; Cano et al., 2019)

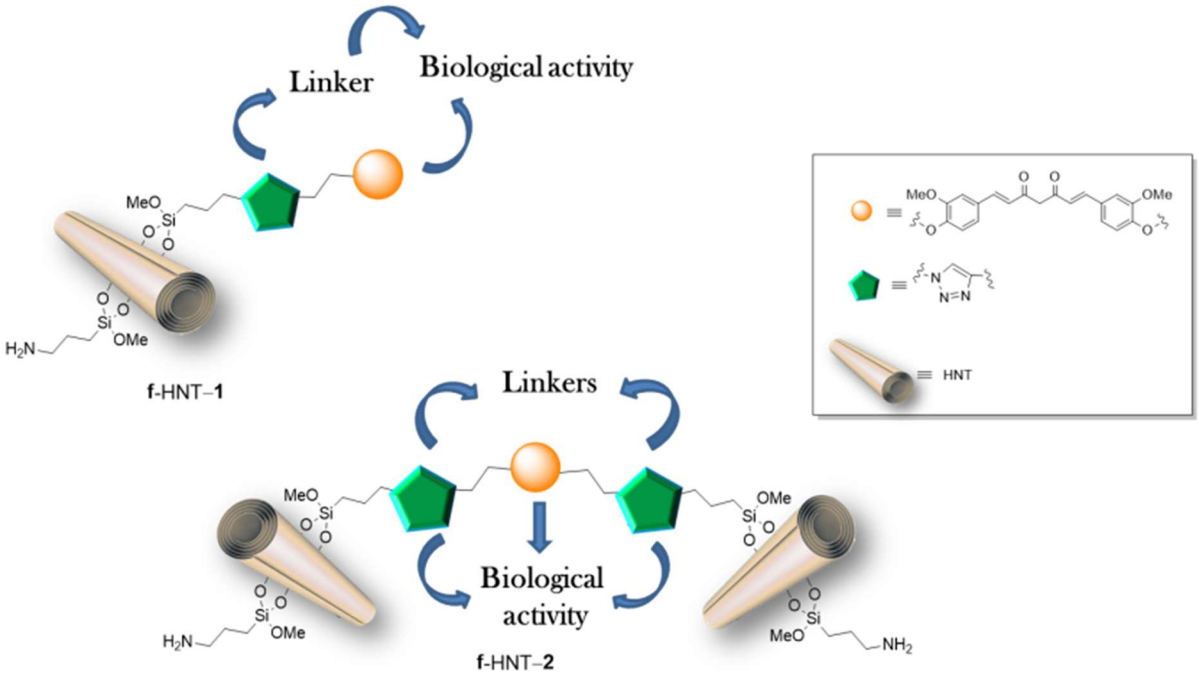

Figure 2. Cartoon representation of the synthetized **f**-HNT–**1** and **2** carrier systems.

Experimental section

Material and methods

All reagents were purchased from Sigma-Aldrich by Merck and used without further purification.

Halloysite was purchased from Sigma-Aldrich by Merck and used without further purification. Halloysite has an average tube diameter of 50 nm and inner lumen diameter of 15 nm. Typical specific surface area is 65 $m^2\ g^{-1}$; pore volume of ~1.25 $cm^3\ g^{-1}$; refractive index 1.54 and specific gravity 2.53 g cm^{-3}.

Microwave-assisted syntheses were carried out with a CEM DISCOVER monomode system in a closed vessel.

Thermogravimetric analyses were performed on a Q5000 IR apparatus (TGA Instruments) under a nitrogen flow of 25 $cm^3\ min^{-1}$ for the sample and 10 $cm^3\ min^{-1}$ for the balance. The weight of each sample was ca. 5 mg. Measurements were carried out by heating the sample from room temperature up to 900 °C at a rate of 10 °C min^{-1}.

IR spectra (KBr) were recorded with an Agilent Technologies Cary 630 FT-IR spectrometer. Specimens for these measurements were prepared by mixing 5 mg of the sample powder with 100 mg of KBr.

An ESEM FEI QUANTA 200 F microscope was used to study the morphology of the functionalized HNTs. Before each experiment, the sample was coated with gold under argon by means of an Edwards Sputter Coater S150A to avoid charging under the electron beam.

TEM images were acquired by an atomic resolution analytical microscope (ARM200F JEOL Ltd, Japan) operating at 200 KeV. All of the images have been acquired in conventional TEM (C/TEM) mode and bright-field mode.

UV-vis measurements were performed using a Beckmann DU 650 spectrometer.

Zetasizer Nano-ZS (Malvern Instruments) apparatus was employed to perform Dynamic light scattering (DLS) and ζ- potential measurements. Both experiments were conducted on aqueous dispersions (concentration = 10^{-3} wt%) at 25.0 ± 0.1 °C. As concerns DLS investigations, the wavelength and the scattering angle were set at 632.8 nm and 173°, respectively. The registered field-time autocorrelation functions were analyzed by using an Inverse La Place Transformation.

The HNT-N_3 nanomaterial, Cur–**1**, Cur–**2** and Cur–**3** were synthetized as previously reported.(Bonaccorsi et al., 2019; Riela et al., 2014)

Syntheses

Synthesis of HNT–1 derivative

HNT-N_3 (50 mg), Cur–**1** (2.5 mg, 6.1×10^{-3} mmol), 1 mg of $CuSO_4\cdot\times 5H_2O$ and 1.5 mg of sodium ascorbate were weighed in a microwave test tube provided with a cup. Afterwards, 1 mL of a mixture $H_2O/^tBuOH$ (1:1) was added and the dispersion was subjected to ultrasound for ca. 1 min. The crude was inserted in the MW apparatus at 100 °C, under constant stirring, for 10 min. Successively, the solid was collected by centrifuge, washed tree times with water and 3 time with CH_2Cl_2 and finally dried at 40 °C under vacuum.

Synthesis of HNT–2 derivative

HNT-N_3 (50 mg), Cur–**2** (10 mg, 2×10^{-2} mmol), 1 mg of $CuSO_4\cdot\times 5H_2O$ and 1.5 mg of sodium ascorbate were weighed in a microwave test tube provided with a cup. Afterwards, 1 mL of a mixture $H_2O/^tBuOH$ (1:1) was added and the dispersion was subjected to ultrasound for ca. 1 min. The crude was inserted in the MW apparatus at 100 °C, under constant stirring, for 10 min. Successively, the solid was collected by centrifuge, washed tree times with water and 3 time with CH_2Cl_2 and finally dried at 40 °C under vacuum.

Synthesis of the f-HNT–1 and f-HNT–2 derivatives

The HNT–**1** or HNT–**2** derivative (30 mg) were suspended in DMF (1 mL) and triphenylphosphine (PPh_3) (15 mg, 7 × 10^{-5} mmol) was added to the reaction mixture under inert atmosphere. The dispersion was left to stir at room temperature for 1 h. After this time a NH_3 aqueous solution (30 μL) was added dropwise. After 5 days the solvent was filtered off and the powder was washed several times with CH_2Cl_2 and finally dried at 50 °C under vacuum.

Synthesis of the HNT/3, f-HNT–4 and 5 supramolecular hybrids

To a dispersion of p-HNT, **f**-HNT–**1** or **2** derivatives in water (5 mL). 1 mL of a solution 10^{-2} M of compound **3** in CH_2Cl_2 was added. The suspension was sonicated for 5 min, at an ultrasound power of 200 W and at 25 °C and then was evacuated for 3 cycles. The suspension was left under stirring for 18 h at room temperature. After this time, the powder was washed with water and then dried at 40 °C.

Synthesis of the f-HNT–6 and 7 supramolecular hybrids

The loading of doxorubicin onto the **f**-HNT–**1** and **f**-HNT–**2** hybrids was carried out by mixing the hybrids with an aqueous doxorubicin solution (3.45×10^{-3} M). Then, the obtained suspension was left to stir at room temperature for ca. 16 h. After loading, the obtained complexes were washed with water in order to remove free Dox. The amount of drug loaded on the HNT hybrids was estimated by UV-vis spectroscopy ate the wavelength of 500 nm by using the Lambert Beer law.

Kinetic Release.

The release of Cur–**3** or Dox from **f**-HNT–**4**, **5**, **6** and **7** nanocomposites was performed as follows: 25 mg of the sample were transferred into a dialysis membrane (Medicell International Ltd MWCO 12-14000 with diameter of 21.5 mm) and wet with 1 mL of phosphate buffer pH 7.4. The membrane was then put in a round bottom flask containing 9 mL of the phosphate buffer at 37 °C and stirred. At fixed times, 1 mL of the release medium was withdrawn and analyzed. To keep constant the volume of the release medium 1 mL of fresh buffer was added each time to replace the withdrawn one. The drug concentration in the solution was determined by UV-vis spectrophotometry using the Lambert-Beer law.
Total amount of drugs released (F_t) was calculated as follows:

$$F_t = V_m C_t + \sum_{i=0}^{t-1} V_a C_i$$

(Eq. 1)

where V_m and C_t are volume and concentration of the drug at time t. V_a is the volume of the sample withdrawn and C_i is drug concentration at time i ($i<t$).

Cells. The human breast cancer cell lines MDA-MB-231 (ATCC®: HTB-26™, Rockville, MD, USA) and SUM149 (SUM149PT—Asterand Bioscience Detroit, MI) were kindly provided by Dr. Elda Tagliabue (Molecular Targeting Unit, Department of Experimental Oncology and Molecular Medicine, Fondazione Institute of Hospitalization and Scientific Care, National Cancer Institute, Milan, Italy) and were authenticated using the short tandem repeat profiling method in their Institute facility.

The HL60 cells were obtained from ATCC® (CCL-240, Rockville, MD, USA), while its variant HL60R, was selected for multidrug resistance (MDR) by exposure to gradually increasing concentrations of doxorubicin and express P-glycoprotein.

After obtaining the cells, the first step carried out was assigned passage number 1. Cells were routinely tested for Mycoplasma contamination and were used for all experiments with a narrow range of passage number (4–6).

MDA-MB-231 cell lines were cultured in Dulbecco's modified Eagle's medium, and SUM 149 cell lines were cultured in Dulbecco's modified Eagle's medium/F-12 supplemented with insulin (5 µg/mL); HL60 and HL60R cell lines were cultured in RPMI 1640. All media were supplemented with 10% heat-inactivated fetal calf serum, 2mMl-glutamine, 100U/mL penicillin, and 100 µg/mL streptomycin (all reagents were from HyClone Europe Ltd, Cramlington, United Kingdom). The cells were cultured in a humidified atmosphere at 37°C in 5% CO_2.

Cell growth assays. The cells were seeded at 2×10^4 cells/well onto 96-well plates and incubated overnight at 37 °C. At time 0, the medium was replaced with fresh complete medium supplemented of HTN- curcumin derivatives. Following 72, 96 or 120 h of treatment, 16 µL of a commercial solution obtained from Promega Corporation (Madison, WI, USA) containing 3-(4,5-dimethylthiazol-2-yl)-5-(3-carboxy methoxyphenyl)-2-(4-sulphophenyl)-2H-tetrazolium (MTS) and phenazine ethosulfate were added. The plates were incubated in a humidified atmosphere at 37 °C in 5% CO_2 for 2 h, and the bioreduction of MTS dye was evaluated by measuring the absorbance of each well at 490 nm using a microplate absorbance reader (iMark Microplate Reader; Bio-Rad Laboratories, Inc., Hercules, CA, USA). Cell growth inhibition was expressed as a percentage (mean ± SD) of the absorbance of the control cells.

Results and Discussion

Multifunctional carrier systems were developed by two synthetic steps: i) first, covalent linkage between Cur–**1** and Cur–**2**(Dolai et al., 2011) and modified HNT(Riela et al., 2014) was performed (**f**-HNT–**1** and **f**-HNT–**2**, respectively); ii) second, Cur–**3**(Barattucci et al., 2018) or Dox were loaded into **f**-HNT–**1** and **f**-HNT–**2** hybrid systems.

The HNT–**1** and HNT–**2** derivatives were obtained according to the synthetic route shown in Scheme 1, using click chemistry, in particular the Huisgen 1,3-dipolar cycloaddition (CuAAC).

Starting from HNT-N_3 (0.5 mmol g^{-1} loading of azido groups) the curcumin derivatives were grafted on their external surface by the CuAAC reaction, obtaining compounds HNT–**1** and HNT–**2**, where curcumins were linked by a triazole ring. The covalent grafting of Cur–**1** and Cur–**2** was carried out by microwave irradiation for 10 min at 100 °C. Then, the obtained nanomaterials were isolated by subsequent washings with H_2O and CH_2Cl_2 in order to remove the catalyst and some residual unreacted reagents. On the basis of the stoichiometric ratios, it should be considered that an excess of unreacted azido groups could be present, and they could be able to undergo further functionalization.

Therefore, the HNT–**1** and HNT–**2** were subjected to post-modification by reduction under the Staudinger reaction conditions (triphenylphosphine, DMF, r.t.) to obtain **f**-HNT–**1** and **f**-HNT–**2**, respectively (Scheme 1).(Cinà et al., 2017)

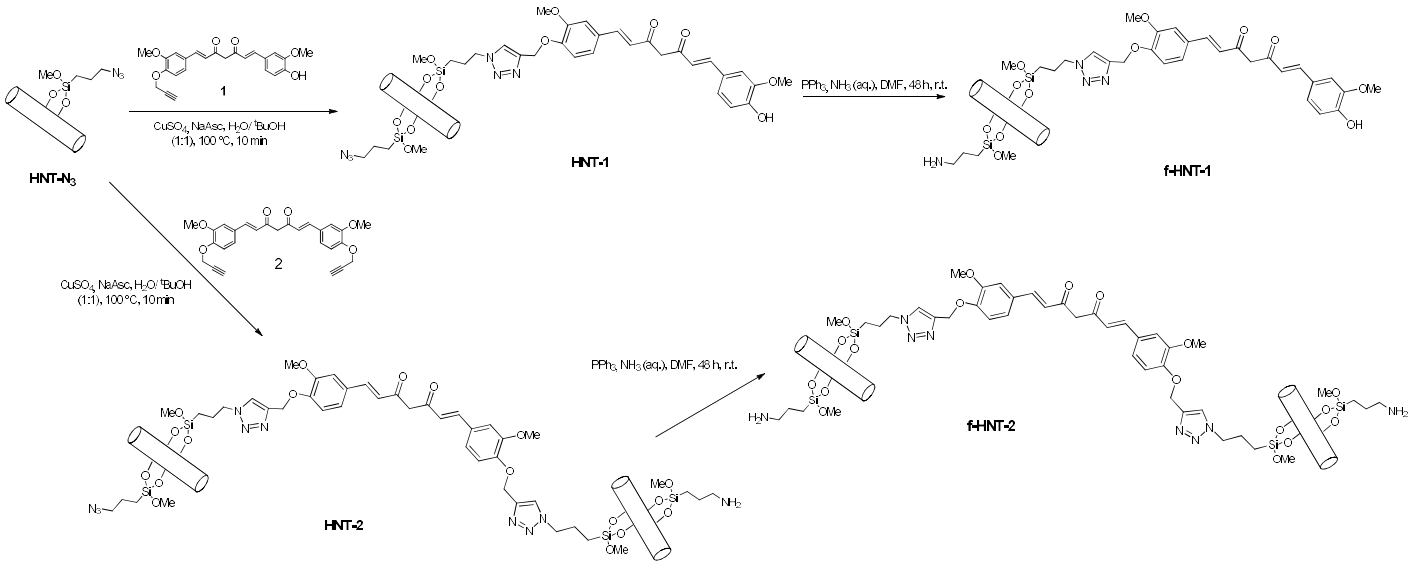

Scheme 1. Schematic representation of the **f**-HNT–**1** and **f**-HNT–**2** derivatives.

The HNT hybrid materials were characterized by several techniques. In Figures 3a-b the FT-IR spectra of the different HNT derivatives and those of Cur–**1** and Cur–**2**, for comparison, are reported.

Compared to the FT-IR spectra of HNT-N_3 and Cur–**1** and Cur–**2** derivatives, the FT-IR spectra of **f**-HNT–**1** and **f**-HNT–**2** exhibit the typical vibration stretching bands of both precursors.(Lopes-Rodrigues et al., 2017; Massaro et al., 2018c) In particular, besides the typical HNT signals, the HNT hybrids show the vibration stretching bands for C–H stretching of methylene groups around 2960 cm^{-1} and 2865 cm^{-1} (Figure 3a-b). Furthermore, bands at ca. 1583, 1508, 1440, 1414 and 1290 cm^{-1} are due to the vibration stretching bands of carbonyl and aromatic groups of curcumin. It is noteworthy that in the FT-IR spectra of HNT–**1** and HNT–**2** an intense signal around 2100 cm^{-1} is visible, due to the presence of the unreacted excess of azido groups (Figure S1). After reduction of the azido groups in HNT–**1** and HNT–**2** by means of PPh_3, the FT-IR of **f**-HNT–**1** and **f**-HNT–**2** exhibited the almost complete disappearance of the $–N_3$ vibration band.

The UV–vis absorption spectra of **f**-HNT–**1** and **f**-HNT–**2** hybrids (Figure 3c) show the successful loading of drug molecules. The ethanolic solution of the hybrids displayed the characteristic absorption of the curcumin derivatives (Cur–**1** and Cur–**2**) at ca. 420 nm.

Thermogravimetric analyses (TGA) were performed on the pristine HNT and on the hybrid derivatives (Figure 3d). Both **f**-HNT–**1** and **f**-HNT–**2** showed similar degradation pathway of pristine HNT except for the thermal degradation of grafted curcumin species. From the mass change values, it is possible to estimate the amount of curcumin species grafted on the HNT surface as ca. 2.2 ± 0.1 and 3.3 ± 0.1 wt% for **f**-HNT–**1** and **f**-HNT–**2**, respectively.

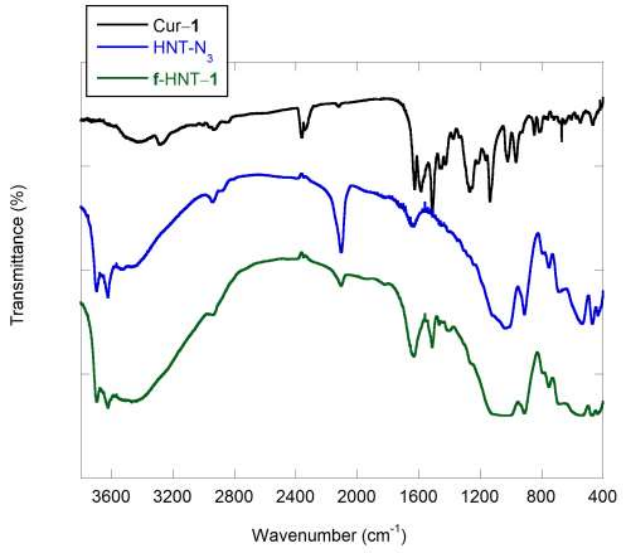

(a)

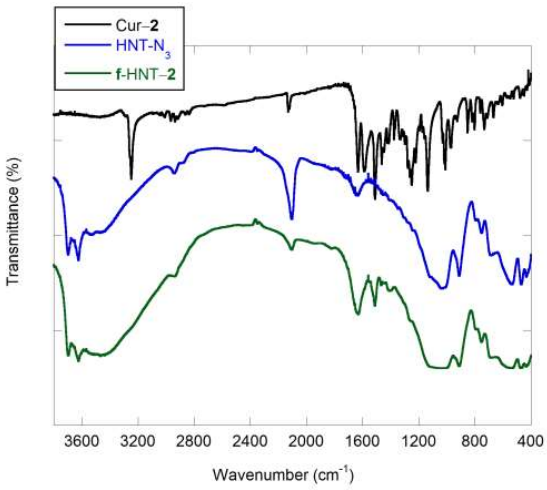

(b)

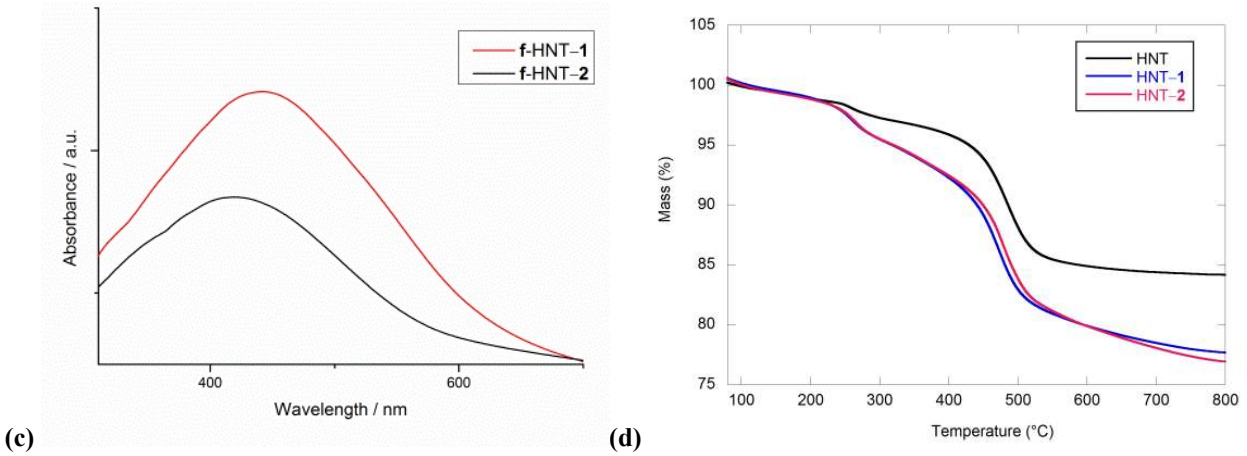

Figure 3. (a-b) FT-IR spectra of HNT-N_3, Cur–**1** and Cur–**2**, **f**-HNT–**1**, **f**-HNT–**2**; (c) UV-vis spectra of **f**-HNT–**1** and **f**-HNT–**2**; (d) thermoanalytical curves of p-HNT, **f**-HNT–**1** and **f**-HNT–**2**.

The diffusion behaviour in water for **f**-HNT–**1** and **f**-HNT–**2** was evaluated by dynamic light scattering (DLS) measurements. The average apparent hydrodynamic diameters are related to the characteristic lengths of the anisotropic particles, as well as to the shell hydration and the aggregation phenomena. It is known from the literature that the apparent hydrodynamic diameter for anisotropic particles is a direct measure of the translational diffusion behaviour of the scattering objects and it can be correlated to the HNT composites actual characteristic sizes.(Cavallaro et al., 2015; Massaro et al., 2015)

In Figure 4, the obtained distribution functions of the average hydrodynamic diameters are reported for **f**-HNT–**1** and **f**-HNT–**2**. The curves clearly show that the average hydrodynamic diameter of **f**-HNT–**1** is slightly lower than that of **f**-HNT–**2**. In detail, the **f**-HNT–**1** shows a distribution of hydrodynamic diameters ranging between 200 and 500 nm centred at ca. 340 nm, that is higher value than pristine nanotubes (typically centred at ca. 250 nm). Conversely, the **f**-HNT–**2** hybrid forms aggregates with an apparent hydrodynamic diameter of ca. 825 nm. Taking into account the molecular structure of the curcumin derivative Cur–**2**, this difference is likely due to the possibility to form a bridge between one curcumin unit and two different nanotubes promoting the aggregation of the tubular nanoparticles.

The effect of the curcumin derivatives grafting on the surface charge of HNTs was investigated by ζ-potential measurements in water. It was found that the ζ-potential values of **f**-HNT–**1** and **f**-HNT–**2** are -15.2 ±0.4 mV and -22.8 ±0.5 mV, respectively. These values show a decrease of the net negative charge compared to that of pristine HNTs (-34.4 mV).(Massaro et al., 2018a) These findings are in agreement with the presence of the amino groups on HNT external surface, which

are protonated in a neutral medium. This result is promising for the use of the nanocomposite in biological field since it can enhance their cellular uptake.

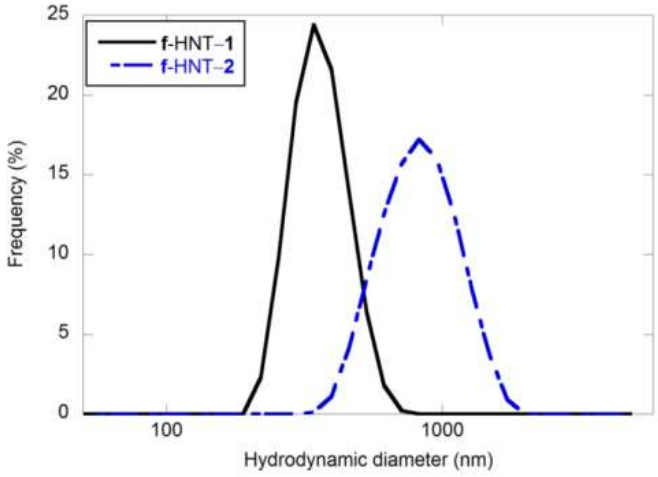

Figure 4. Distribution functions of apparent hydrodynamic diameters for **f**-HNT–**1** and **f**-HNT–**2**.

The surface morphology of the **f**-HNT–**1** and **f**-HNT–**2** was imaged by SEM and TEM (Figure 5). From SEM and TEM images, it clearly appears that the tubular shape of the halloysite is maintained after grafting of curcumin derivatives (Figure 5). Furthermore, the SEM images show that **f**-HNT–**1** and **f**-HNT–**2** have a rather compact structure where nanotubes seem to be glued together as a result of interactions established by the organic structures grafted on the external surface (presumably π–π interactions among the different aromatic rings) (Figures 5a-b).

TEM micrographies (Figure 5c-d) clearly show the different morphologies of nanocomposites obtained by grafting the Cur–**1** and Cur–**2** on HNT external surface. Indeed, in the case **f**-HNT–**1** we observe a single tube covered by a sheet of organic moiety (red arrows in Figure 5c), on the contrary, in **f**-HNT–**2** hybrid, the tubes are aggregated according to the curcumin bridged among the different nanotubes (yellow arrow in Figure 5d) with some free organic units (white arrow in Figure 5d). These findings are in agreement with the above discussed DLS data.

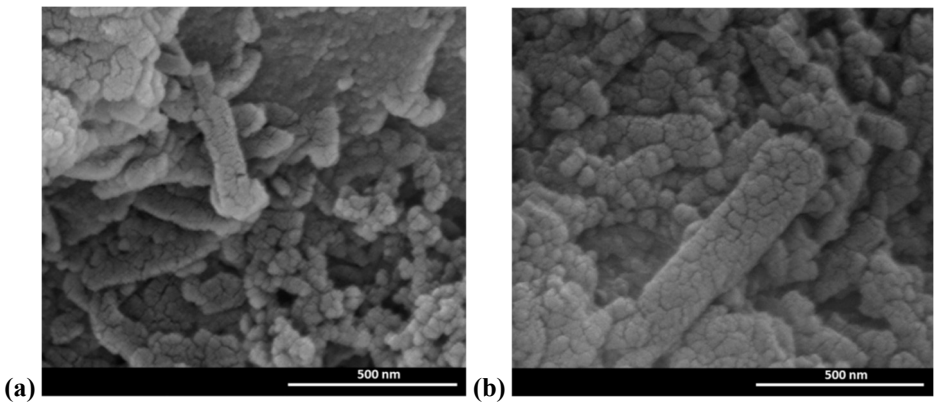

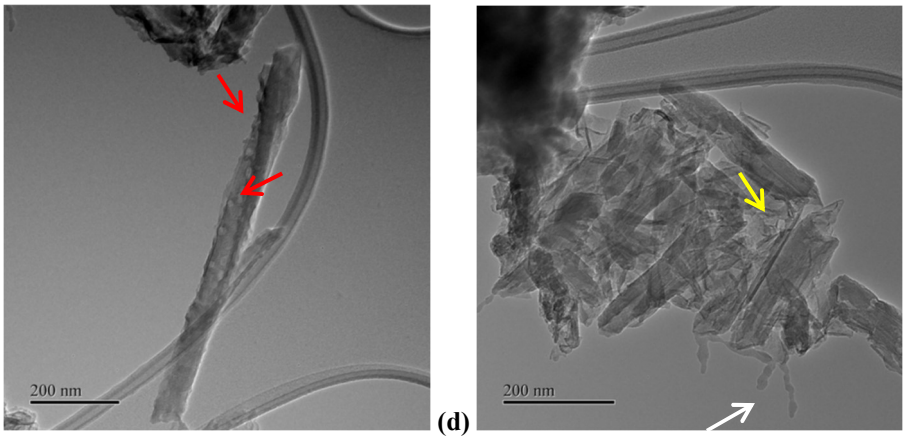

Figure 5. (a-b) SEM images and (c-d) TEM images of (a-c) **f**-HNT–**1**; (b-d) **f**-HNT–**2**.

With the aim of combining two or more biologically active molecules with synergistic effects, we loaded the multifunctional carriers with Cur–**3**. In addition, to enhance the antitumoral effects of the HNT-Cur derivatives and to limit some side effects, similar hybrid complexes were prepared by loading doxorubicin (Dox) onto the HNT hybrid.

Preliminary studies performed in order to investigate the loading ability of pristine HNT towards Cur–**3** have shown that it can efficiently interact with the HNT lumen (HNT/**3**) with a loading percent, estimated by TGA, of 3.6 wt% (see SI).

Therefore, on the basis of these findings, a step further was addressed to load Cur–**3** or Dox into **f**-HNT–**1** and **f**-HNT–**2** to obtain **f**-HNT–**4**, **5**, **6** and **7** nanocomposites, respectively (Scheme 2)**.**

The loading of Cur–**3** and Dox in **f**-HNT–**4**, **5**, **6** and **7** was investigated by thermogravimetry analysis which has shown a loading of 6.5 and 9 wt% for Cur–**3** (into **f**-HNT–**4** and **5**, respectively**)** and ca. 1 wt% for Dox (into **f**-HNT–**6** and **7**, respectively**)** with an entrapment efficiency of 100% in all cases. The higher value loading of Cur–**3** obtained in **f**-HNT–**4** and **5**, with respect to that in pristine HNT (3.6 wt%) could be ascribed to the presence of Cur–**3** molecules both loaded into HNT lumen and supramolecular interacting with the modified HNT external surface.

As far as the Dox loading is concerned, the obtained low value is in agreement with our choice to incorporate a small amount of such, toxic and with numerous side effects, drug.

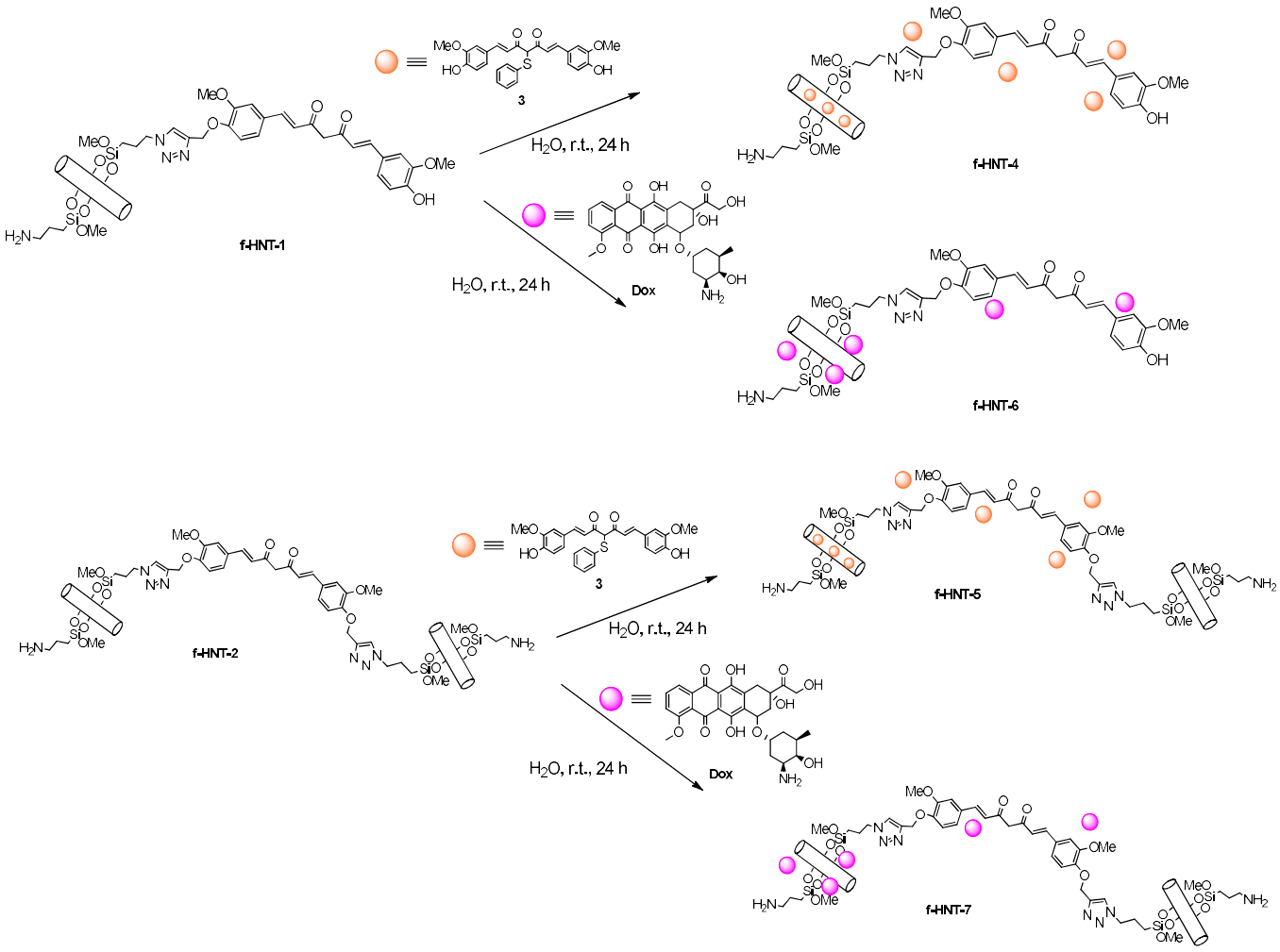

Scheme 2. Schematic representation of the synthesis of **f**-HNT–**4, 5, 6** and **7** nanocomposites.

Kinetic Release

To evaluate the performances of the hybrid systems for application in the drug carrier field, the kinetic release of Cur–**3** and Dox drugs from HNT hybrid systems was evaluated by the dialysis bag method using conditions designed to mimic physiological conditions (phosphate buffer pH 7.4) and the obtained kinetic data are shown in Figure 6.

Noteworthy, in these conditions **f**-HNT–**4** and **5** retain almost the total amount of the loaded curcumin for at least 60 h. These results are similar to that obtained from a carrier system where some triazolium salt units are covalently grafted to HNT,**(Riela et al., 2014)** indicating an interaction existing by the Cur–**3** and the halloysite modified external surface, according to TGA data.

On the contrary, the Dox molecules showed a most rapid release from **f**-HNT–**6** and **7** as a consequence of a more aqueous solubility of doxorubicin with respect to Cur–**3**. The release profile

showed that, after 24 h, ca. 65 wt% and 94 wt% of doxorubicin was released from **f**-HNT–**6** and **7**, respectively.

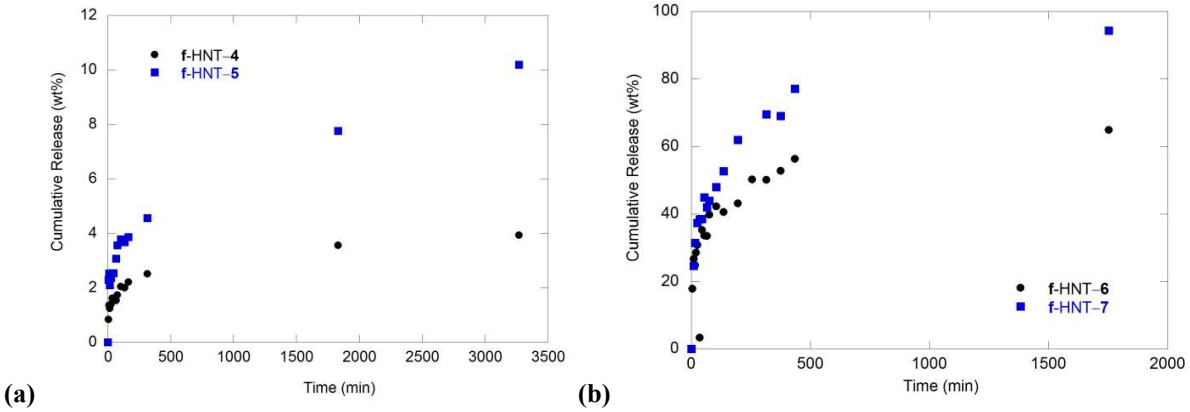

Figure 6. Kinetic release of (a) Cur–**3** from **f**-HNT–**4** and **5** and (b) Dox from **f**-HNT–**6** and **7** in phosphate buffer pH 7.4 at 37 °C.

The kinetic data obtained were analyzed by double exponential (DEM) and Korsmeyer–Peppas models to deep investigate the release behavior of Cur–**3** and Dox from such complex systems. The results showed that data well fitted for each case investigated (Table 1). According to the literature, the DEM describes a mechanism consisting of two parallel reactions involving two distinguishable species. Therefore, in our case we observed the release of Cur–**3** and Dox from two different adsorption sites.

On the basis of the above results, it is possible to conclude that the interaction among Cur–**3** and Cur–**1** and Cur–**2** linked on HNT surface are so strong to inhibit the release of the supramolecular linked Curc–**3**. On the contrary, desorption of Dox molecules, physically adsorbed onto the HNT surface, is a consequence of the less affinity that these molecules show for Cur derivatives respect to that for aqueous environment.

Table 1. Kinetic parameters for Cur–**3** and Dox release from **f**-HNT–**4**, **5**, **6** and **7** nanocomposites.

	DEM			Power Fit		
	k_1 (min^{-1})	k_2 (min^{-1})	R^2	k (min^{-1})	n	R^2
f-HNT–**4**	0.20 ± 0.04	0.0019 ± 0.0003	0.990	0.72 ± 0.03	0.211 ± 0.007	0.988
f-HNT–**5**	0.5 ± 0.3	0.0011 ± 0.0002	0.982	0.96 ± 0.08	0.28 ± 0.01	0.976
f-HNT–**6**	0.14 ± 0.04	0.0028 ± 0.0005	0.970	14.6 ± 5.7	0.21 ± 0.05	0.829
f-HNT–**7**	0.13 ± 0.02	0.0028 ± 0.0002	0.993	17.2 ± 2.5	0.23 ± 0.02	0.982

In vitro cytotoxicity assay

The cytotoxicity of the different HNT hybrids (**f**-HNT–**1**, **2**, **4**, **5**, **6** and **7**) and the HNT/**3** complex on two triple negative breast cancer cell lines, SUM 149 and MDA-MB-231 and on two acute

myeloid leukemia cell lines, HL60 and its multidrug resistant variant HL60R are summarized in Table 2.

As expected, in all cell lines investigated, the HNT/Cur-**3** complex (entry 1) did not show any cytotoxic effects, as a consequence of the low availability of the Cur–**3** due to its strong interaction with halloysite lumen.(Riela et al., 2014)

On the contrary, **f**-HNT–**1** and **2** derivatives reached the IC_{50} in all cell lines (entries 2-3); in particular **f**-HNT–**2** hybrid is more active than Cur–**2**.(Bonaccorsi et al., 2019) This latter result is in agreement with the synthetic procedure adopted for the covalent linkage of Cur–**2** on HNT external surface. Indeed, after the CuAAC reaction between Curc–**2** and the azido functionalized HNT, a triazole unit was introduced onto the carrier, which can afford a synergistic effect owing to its very interesting biological activities, in particular antitumoral effects.(Riela et al., 2014)

Both **f**-HNT–**1** and **2** resulted promising on the HL60 and HL60R. Noteworthy, increased antitumor activity was found with the compound **f**-HNT–**1** on HL60R cell line compared to the parental HL60. This result is worthy of further investigations to evaluate the capacity of **f**-HNT–**1** to interfere with molecular mechanisms of multidrug resistance. The dual drug loaded systems (entries 4-5), **f**-HNT–**4** and **5** showed different results. In SUM 149 cells, **f**-HNT–**4** had a IC_{50} clearly lower than the precursor (**f**-HNT–**1)**, in particular at 24 and 20 μM after 96 h and 120 h of treatment, respectively; in the same cell line, on the contrary, **f**-HNT–**5** reached the IC_{50} at 50 μM after 96 h of treatment.

In MDA-MB-231 cells both **f**-HNT–**4** and **5** were more cytotoxic than **f**-HNT–**1** and **2** hybrids. In particular, the IC_{50} values for **f**-HNT–**1** were 19 and 5 μM after 96 h and 120 h of treatment, respectively; while IC_{50} values for **f**-HNT–**2** were 9 and 10 μM after 96 h and 120 h of treatment, respectively. Therefore, the

multifunctional systems (**f**-HNT–**4** and **5**) compared to pristine components (Cur–**1** and **2**(Bonaccorsi et al., 2019) and **f**-HNT–**1** and **2**), showed significant improvement in the cellular cytotoxicity as a consequence of synergistic effect showed by the co-delivery of two different curcumin species.

To the light of the above results, it seems clear that the difference in the efficacy of different HNT hybrids could be associated with the availability of the curcumin derivatives to act as anticancer drug. This means that the antiproliferative activity was correlated both to the release profile of Curc-**3** from HNT hybrids, and to the size of the final hybrids obtained. It is known that cellular uptake of complex nanoparticles is strictly correlated to the particle size, small particles showing higher cellular internalization, localization and cytotoxicity with respect to the larger ones.

The *in vitro* kinetic release demonstrated that Curc-**3** is slowly released from the HNT hybrids over the time, in physiological conditions. DLS measurements confirm that the size of the **f**-HNT–**4** and **5** is the driving force in the cellular uptake. Indeed, we found that **f**-HNT–**4** and **5** possess hydrodynamic diameters larger than 1000 nm. These results are in agreement with the low cytotoxicity observed for HL60 and HL60R cell lines. In this case, we hypothesize a failed entry of **f**-HNT–**4** and **5** into the cells for both their size, greater than f-HNT–**1** and **2**, and the small size of the HL60 and HL60R cells.

To improve the cytotoxic effect of the **f**-HNT–**1** and **2** hybrids towards acute myeloid leukemia cell lines, we finally tested the **f**-HNT–**6** and **7** (entries 6-7). Both hybrids showed improved antiproliferative activities with respect to the precursors (**f**-HNT–**1** and **2**), in particular, as concern the HL60 cells, they resulted very cytotoxic at low concentrations (IC_{50} of 16 and 14.5 μM for **f**-HNT–**6** and **7**, respectively).

However, also in this case, the presence of doxorubicin did not significant improve the cytotoxicity on the multidrug resistant variant HL60R, actually in the case of **f**-HNT–**7**, it results worse than the ones obtained in the presence of the alone **f**-HNT–**2**.

Table 2. IC_{50} values of the HNT hybrid systems investigated on the different cell lines.

Entry		SUM 149 (μM)	MDA-MB-231 (μM)	HL60 (μM)	HL60 R (μM)
1	HNT/**3**	IC_{50} not reached	IC_{50} not reached	IC_{50} not reached	IC_{50} not reached
2	**f**-HNT–**1**	68.0 ± 15.5	75.0 ± 8.1	35.0 ± 3.5	21.0 ± 2.1
3	**f**-HNT–**2**	11.5± 1.8	13.0 ± 0.3	7.0 ± 0.0	8.0 ± 0.0
4	**f**-HNT–**4**	24 (96 h)/ 20 (120 h)	19 (96 h)/ 5 (120 h)	IC_{50} not reached	IC_{50} not reached
5	**f**-HNT–**5**	50 (96 h)/ 20 (120 h)	9 (96 h)/ 10 (120 h)	IC_{50} not reached	IC_{50} not reached
6	**f**-HNT–**6**			16	IC_{50} not reached
7	**f**-HNT–**7**			14.5	21.5

Conclusions

In this study we have synthetized two new halloysite nanotubes covalently linked, by triazole units, at curcumin derivatives that possesses one or two terminal alkyne groups.

The new nanomaterials were characterized by several techniques that confirm the functionalization of the tubes. In particular TEM images clearly show the different morphologies obtained for the two hybrids; one where the curcumin derivative is linked as single molecule on HNT external surface, the other where the curcumin is bridged between two different HNTs.

To exploit synergistic effects among different drugs, we also loaded, on the carrier systems obtained, another curcumin derivative or doxorubicin and we tested the complexes synthetized against four different cancer cell lines, namely two triple negative breast cancer cell lines, SUM 149 and MDA-MB-231 and on two acute myeloid leukemia cell lines, HL60 and its multidrug resistant variant HL60R. The obtained results show that the cytotoxicity effects of the hybrids are strictly correlated both to the nanoparticles size and to the release profile of the drug supramolecularly loaded on HNT surfaces.

The new synthetic approach presented herein envisages the development of a carrier system with possesses both curcumin and triazole units covalently linked on halloysite external surface to obtain a dual drug carrier system. In addition the presence of the empty halloysite lumen allows us to load another biological molecule to exploit synergistic effects for cancer treatment. These systems conversely to previous studies present in the literature(Massaro et al., 2016a; Riela et al., 2014) possess enhanced antiproliferative activities even on multidrug resistant cancer cells.

Future work will be devoted to further in vitro and in vivo studies to assess the feasibility of the novel systems in order to overcome the multidrug resistance, often associated with the chemodrugs administration and to limit the severe side effects associated to them, increasing the patience compliance.

Acknowledgements

This project has received funding from the European Union's Horizon 2020 research and innovaPon programme under grant agreement No 823717 – ESTEEM3. The work was carried out in the frame of the PON "AIM: Attrazione e Mobilità Internazionale" No. 1808223-2 project.

References

Babos, G., Biró, E., Meiczinger, M., Feczkó, T., 2018. Dual Drug Delivery of Sorafenib and Doxorubicin from PLGA and PEG-PLGA Polymeric Nanoparticles. Polymers 10, 895.

Barattucci, A., Aversa, M.C., Mancuso, A., Salerno, T.M.G., Bonaccorsi, P., 2018. Transient Sulfenic Acids in the Synthesis of Biologically Relevant Products. Molecules 23, 1030.

Bellani, L., Giorgetti, L., Riela, S., Lazzara, G., Scialabba, A., Massaro, M., 2016. Ecotoxicity of halloysite nanotube–supported palladium nanoparticles in Raphanus sativus L. Environ. Toxicol. Chem. 35, 2503-2510.

Bergaya, F., Lagaly, G., 2006. Chapter 1 General Introduction: Clays, Clay Minerals, and Clay Science, Developments in Clay Science, pp. 1-18.

Bonaccorsi, P.M., Labbozzetta, M., Barattucci, A., Salerno, T., Poma, P., Notarbartolo, M., 2019. Synthesis of curcumin derivatives and analysis of their antitumoral effects in triple negative breast cancer (TNBC) cell lines. Bioorg. Med. Chem. Lett. Submitted.

Cano, A., Ettcheto, M., Chang, J.-H., Barroso, E., Espina, M., Kühne, B.A., Barenys, M., Auladell, C., Folch, J., Souto, E.B., Camins, A., Turowski, P., García, M.L., 2019. Dual-drug loaded nanoparticles of Epigallocatechin-3-gallate (EGCG)/Ascorbic acid enhance therapeutic efficacy of EGCG in a APPswe/PS1dE9 Alzheimer's disease mice model. J. Controlled Release 301, 62-75.

Cavallaro, G., Lazzara, G., Massaro, M., Milioto, S., Noto, R., Parisi, F., Riela, S., 2015. Biocompatible Poly(N-isopropylacrylamide)-halloysite Nanotubes for Thermoresponsive Curcumin Release. J. Phys. Chem. C 119, 8944-8951.
Cinà, V., Russo, M., Lazzara, G., Chillura Martino, D., Lo Meo, P., 2017. Pre- and post-modification of mixed cyclodextrin-calixarene co-polymers: A route towards tunability. Carbohydr. Polym. 157, 1393-1403.
Dolai, S., Shi, W., Corbo, C., Sun, C., Averick, S., Obeysekera, D., Farid, M., Alonso, A., Banerjee, P., Raja, K., 2011. "Clicked" Sugar–Curcumin Conjugate: Modulator of Amyloid-β and Tau Peptide Aggregation at Ultralow Concentrations. ACS Chem. Neurosci. 2, 694-699.
Fakhrullin, R.F., Lvov, Y.M., 2016. Halloysite clay nanotubes for tissue engineering. Nanomedicine 11, 2243-2246.
Fakhrullina, G.I., Akhatova, F.S., Lvov, Y.M., Fakhrullin, R.F., 2015. Toxicity of halloysite clay nanotubes in vivo: a Caenorhabditis elegans study. Environ. Sci. Nano 2, 54-59.
Fan, L., Zhang, J., Wang, A., 2013. In situ generation of sodium alginate/hydroxyapatite/halloysite nanotubes nanocomposite hydrogel beads as drug-controlled release matrices. J. Mater. Chem. B 1, 6261-6270.
Kryuchkova, M., Danilushkina, A.A., Lvov, Y.M., Fakhrullin, R.F., 2016. Evaluation of toxicity of nanoclays and graphene oxide in vivo: a Paramecium caudatum study. Environ. Sci. Nano 3, 442-452.
Lin, J.-T., Ye, Q.-B., Yang, Q.-J., Wang, G.-H., 2019. Hierarchical bioresponsive nanocarriers for codelivery of curcumin and doxorubicin. Colloids Surf. B. Biointerfaces 180, 93-101.
Lopes-Rodrigues, V., Oliveira, A., Correia-da-Silva, M., Pinto, M., Lima, R.T., Sousa, E., Vasconcelos, M.H., 2017. A novel curcumin derivative which inhibits P-glycoprotein, arrests cell cycle and induces apoptosis in multidrug resistance cells. Biorg. Med. Chem. 25, 581-596.
Lvov, Y., Aerov, A., Fakhrullin, R., 2014. Clay nanotube encapsulation for functional biocomposites. Adv. Colloid Interface Sci. 207, 189-198.
Ma, W., Guo, Q., Li, Y., Wang, X., Wang, J., Tu, P., 2017. Co-assembly of doxorubicin and curcumin targeted micelles for synergistic delivery and improving anti-tumor efficacy. Eur. J. Pharm. Biopharm. 112, 209-223.
Massaro, M., Amorati, R., Cavallaro, G., Guernelli, S., Lazzara, G., Milioto, S., Noto, R., Poma, P., Riela, S., 2016a. Direct chemical grafted curcumin on halloysite nanotubes as dual-responsive prodrug for pharmacological applications. Colloids Surf. B. Biointerfaces 140, 505-513.
Massaro, M., Barone, G., Biddeci, G., Cavallaro, G., Di Blasi, F., Lazzara, G., Nicotra, G., Spinella, C., Spinelli, G., Riela, S., 2019a. Halloysite nanotubes-carbon dots hybrids multifunctional nanocarrier with positive cell target ability as a potential non-viral vector for oral gene therapy. J. Colloid Interface Sci. 552, 236-246.
Massaro, M., Buscemi, G., Arista, L., Biddeci, G., Cavallaro, G., D'Anna, F., Di Blasi, F., Ferrante, A., Lazzara, G., Rizzo, C., Spinelli, G., Ullrich, T., Riela, S., 2019b. Multifunctional Carrier Based on Halloysite/Laponite Hybrid Hydrogel for Kartogenin Delivery. ACS Med. Chem. Lett. 10, 419-424.
Massaro, M., Cavallaro, G., Colletti, C.G., D'Azzo, G., Guernelli, S., Lazzara, G., Pieraccini, S., Riela, S., 2018a. Halloysite nanotubes for efficient loading, stabilization and controlled release of insulin. J. Colloid Interface Sci. 524, 156-164.
Massaro, M., Cavallaro, G., Colletti, C.G., Lazzara, G., Milioto, S., Noto, R., Riela, S., 2018b. Chemical modification of halloysite nanotubes for controlled loading and release. J. Mater. Chem. B 6, 3415-3433.
Massaro, M., Colletti, C.G., Fiore, B., La Parola, V., Lazzara, G., Guernelli, S., Zaccheroni, N., Riela, S., 2019c. Gold nanoparticles stabilized by modified halloysite nanotubes for catalytic applications. Appl. Organomet. Chem. 33.
Massaro, M., Colletti, C.G., Guernelli, S., Lazzara, G., Liu, M., Nicotra, G., Noto, R., Parisi, F., Pibiri, I., Spinella, C., Riela, S., 2018c. Photoluminescent hybrid nanomaterials from modified halloysite nanotubes. J. Mater. Chem. C 6, 7377-7384.
Massaro, M., Colletti, C.G., Lazzara, G., Riela, S., 2018d. The use of some clay minerals as natural resources for drug carrier applications. J. Funct. Biomater. 9.
Massaro, M., Piana, S., Colletti, C.G., Noto, R., Riela, S., Baiamonte, C., Giordano, C., Pizzolanti, G., Cavallaro, G., Milioto, S., Lazzara, G., 2015. Multicavity halloysite–amphiphilic cyclodextrin hybrids for co-delivery of natural drugs into thyroid cancer cells. J. Mater. Chem. B 3, 4074-4081.

Massaro, M., Riela, S., Cavallaro, G., Colletti, C.G., Milioto, S., Noto, R., Lazzara, G., 2016b. Ecocompatible Halloysite/Cucurbit[8]uril Hybrid as Efficient Nanosponge for Pollutants Removal. ChemistrySelect 1, 1773-1779.
Paci, A., Veal, G., Bardin, C., Levêque, D., Widmer, N., Beijnen, J., Astier, A., Chatelut, E., 2014. Review of therapeutic drug monitoring of anticancer drugs part 1 – Cytotoxics. Eur. J. Cancer 50, 2010-2019.
Pourjavadi, A., Asgari, S., Hosseini, S.H., Akhlaghi, M., 2018. Codelivery of Hydrophobic and Hydrophilic Drugs by Graphene-Decorated Magnetic Dendrimers. Langmuir 34, 15304-15318.
Riela, S., Massaro, M., Colletti, C.G., Bommarito, A., Giordano, C., Milioto, S., Noto, R., Poma, P., Lazzara, G., 2014. Development and characterization of co-loaded curcumin/triazole-halloysite systems and evaluation of their potential anticancer activity. Int. J. Pharm. 475, 613-623.
Wang, X., Gong, J., Gui, Z., Hu, T., Xu, X., Halloysite nanotubes-induced Al accumulation and oxidative damage in liver of mice after 30-day repeated oral administration. Environ. Toxicol. 0.
Yendluri, R., Otto, D.P., De Villiers, M.M., Vinokurov, V., Lvov, Y.M., 2017. Application of halloysite clay nanotubes as a pharmaceutical excipient. Int. J. Pharm. 521, 267-273.
Zhang, Y., Duan, J., Cai, L., Ma, D., Xue, W., 2016. Supramolecular Aggregate as a High-Efficiency Gene Carrier Mediated with Optimized Assembly Structure. ACS Appl. Mater. Interf. 8, 29343-29355.